

P. Comodi · M. Drábek · M. Montagnoli  
M. Rieder · Z. Weiss · P. F. Zanazzi

## Pressure-induced phase transition in synthetic trioctahedral Rb-mica

Received: 21 October 2002 / Accepted: 25 February 2003

**Abstract** The crystal structure of a synthetic Rb analog of tetra-ferri-annite (Rb-TFA) 1M with the composition  $\text{Rb}_{0.99}\text{Fe}^{2+}_{3.03}(\text{Fe}^{3+}_{1.04}\text{Si}_{2.96})\text{O}_{10.0}(\text{OH})_{2.0}$  was determined by the single-crystal X-ray diffraction method. The structure is homooctahedral (space group  $C2/m$ ) with M1 and M2 occupied by divalent iron. Its unit cell is larger than that of the common potassium trioctahedral mica, and similar lateral dimensions of the tetrahedral and octahedral sheets allow a small tetrahedral rotation angle  $\alpha = 2.23(6)^\circ$ . Structure refinements at 0.0001, 1.76, 2.81, 4.75, and 7.2 GPa indicate that in some respects the Rb-TFA behaves like all other micas when pressure increases: the octahedra are more compressible than the tetrahedra and the interlayer is four times more compressible than the 2:1 layer. However, there is a peculiar behavior of the tetrahedral rotation angle  $\alpha$ : at lower pressures (0.0001, 1.76, 2.81 GPa), it has positive values that increase with pressure [from  $2.23(6)^\circ$  to  $6.3(4)^\circ$ ] as in other micas, but negative values  $-7.5(5)^\circ$  and  $-8.5(9)^\circ$  appear at higher pressures, 4.75 and 7.2 GPa, respectively. This structural evidence, to-

gether with electrostatic energy calculations, shows that Rb-TFA has a Franzini A-type 2:1 layer up to at least 2.81 GPa that at higher pressure yields to a Franzini B-type layer, as shown by the refinements at 4.75 and 7.2 GPa. The inversion of the  $\alpha$  angle is interpreted as a consequence of an isosymmetric displacive phase transition from A-type to B-type structure between 2.81 and 4.75 GPa. The compressibility of the Rb-TFA was also investigated by single-crystal X-ray diffraction up to a maximum pressure of 10 GPa. The lattice parameters reveal a sharp discontinuity between 3.36 and 3.84 GPa, which was associated with the phase transition from Franzini-A to Franzini-B structure.

**Keywords** Mica · Crystal structure · Compressibility · Pressure · Phase transition · X-ray diffraction

### Introduction

Synthetic materials with mica structure can accommodate large cations in the interlayer. Therefore, they have been proposed as possible candidates to host waste storage elements of industrial or nuclear origin. For example, Cs-tetra-ferri-annite 1M was recently synthesized under hydrothermal conditions (Drábek et al. 1998). Its structure was described by Mellini et al. (1996) and its behavior at high pressure and high temperature (Comodi et al. 1999) shows that it is a suitable candidate for the storage of  $^{135}\text{Cs}$  and  $^{137}\text{Cs}$  isotopes. Here we report new structural data on an analogous compound, Rb-tetra-ferri-annite (Rb-TFA from now on), at ambient conditions and a set of five refinements under high-pressure conditions in the diamond anvil cell (DAC) in the range 0.0001–10 GPa. This mica is a stable phase and appears to be a good candidate to accommodate Rb in the interlayer. Furthermore, this study allows a comparison of structural features and compressibility of several dioctahedral and trioctahedral micas containing interlayer cations with different ionic radii.

*Electronic Supplementary Material.* Table 3 have been deposited in electronic form and can be obtained from <http://link.springer.de/link/service/journals/00269>

P. Comodi · M. Montagnoli · P. F. Zanazzi (✉)  
Dipartimento di Scienze della Terra,  
Università di Perugia, Piazza Università, 06100 Perugia, Italy  
e-mail: zanazzi@unipg.it  
Fax: +39-075-5852603  
Tel.: +39-075-5852612

M. Drábek  
Czech Geological Survey, Geologická 6,  
15200 Praha 5, Czech Republic

M. Rieder  
Institute of Geochemistry, Mineralogy and Mineral Resources,  
Charles University, Albertov 6, 12843 Praha 2, Czech Republic

Z. Weiss  
Institute of Materials Chemistry, Technical University Ostrava,  
70833 Ostrava-Poruba, Czech Republic

**Table 1** Conditions of the data collection and refinement of the crystal structure

| <i>P</i> (GPa)       | 0.0001 <sup>a</sup> | 0.0001 <sup>b</sup> | 1.76     | 2.81     | 4.75     | 7.2      |
|----------------------|---------------------|---------------------|----------|----------|----------|----------|
| Total reflections    | 1468                | 1283                | 1095     | 1045     | 1012     | 968      |
| Unique reflections   | 749                 | 409                 | 277      | 193      | 186      | 222      |
| Observed reflections | 533                 | 192                 | 210      | 147      | 142      | 103      |
| Parameters           | 60                  | 27                  | 27       | 27       | 27       | 27       |
| R <sub>eq</sub> %    | 1.8                 | 4.7                 | 9.2      | 9.5      | 9.7      | 10.5     |
| R%                   | 2.5                 | 4.8                 | 6.5      | 6.8      | 7.6      | 7.8      |
| Scan speed           | 0.4                 | 0.06                | 0.06     | 0.06     | 0.06     | 0.04     |
| Scan width           | 2.6                 | 2.6                 | 2.6      | 2.6      | 2.6      | 3.0      |
| Scan type            | $\omega$            | $\omega$            | $\omega$ | $\omega$ | $\omega$ | $\omega$ |
| $\theta$ range (°)   | 3–30                | 3–35                | 3–35     | 3–35     | 3–35     | 3–35     |

<sup>a</sup> Data collected in air<sup>b</sup> Data collected under room conditions in the DAC

## Experimental

Rb–TFA was synthesized under hydrothermal conditions, in sealed metal capsules in standard cold-seal bombs under hydrostatic pressure of 0.1 GPa, at temperature up to 700 °C. The runs were not buffered with respect to oxygen. These conditions were similar to those used for the synthesis of the Cs trioctahedral mica (Drábek et al. 1998). Several dark brown crystals of the Rb–TFA, grown in a temperature-gradient experiment, were analyzed on a JEOL electron microscope equipped with a wavelength-dispersive spectrometer, using synthetic RbAlSiO<sub>4</sub> as a standard for rubidium, fayalite for iron, and kyanite for aluminum and silicon. When calculating its formula, iron was split into divalent and trivalent so that all tetrahedral Fe was trivalent and the total of 22+ charges was maintained. The resulting formula is Rb<sub>0.99</sub>Fe<sup>2+</sup><sub>3.03</sub>(Fe<sup>3+</sup><sub>1.04</sub>Si<sub>2.96</sub>)O<sub>10.0</sub>(OH)<sub>2.0</sub>.

An untwinned crystal from the charge, with dimensions 0.15 × 0.10 × 0.04 mm, was used for diffraction work and mounted on a four-circle Philips PW1100 diffractometer. Integrated intensities for the structure refinement were collected under room conditions using graphite monochromatized MoK $\alpha$  radiation ( $\lambda = 0.7107$  Å). The data come from two equivalent reciprocal lattice quadrants, with indices  $\pm hkl$  and  $\pm \bar{h}\bar{k}l$  in the  $\theta$  range 3–30°. The data were corrected for absorption according to the method of North et al. (1968) and merged. Starting from atomic parameters of the Cs-tetra-ferri-annite (Comodi et al. 1999), anisotropic refinement in the space group *C2/m* was carried out using the SHELXL97 program (Sheldrick 1997), refining against the squared structure factors. Neutral atomic scattering factor values and correction factors for anomalous dispersion were taken from the International tables for X-ray crystallography (Ibers and Hamilton 1974). For the tetrahedral T site, a mixed curve of silicon and iron was employed, allowing a variation of the Si/Fe occupancy ratio. Details of the refinement and data collection are listed in Table 1. Final atomic coordinates and displacement parameters are listed in Table 2; observed and calculated structure factors appear in Table 3.<sup>1</sup>

### High-pressure experiments

A Merrill-Bassett DAC with 1/8 carat diamonds was used for the high-pressure study, with a methanol-ethanol 4:1 mixture as pressure-transmitting medium, and a steel foil, 250  $\mu$ m thick, as gasket material. A small chip of quartz and a powder of BaFCl doped with samarium were mounted together with the sample. Pressure was monitored by measuring the wavelength shift of the fluorescence line at 6876 Å of Sm<sup>2+</sup> (Sm<sup>2+</sup>:BaFCl) (Comodi and Zanazzi 1993) and through the equation of state of quartz (Angel et al. 1997). The uncertainty in the measurement of pressure is 0.05 GPa. Lattice parameters were determined at pressures ranging between 0.0001 and 10 GPa (Table 4) by applying the least-squares method to  $2\theta$  angles of about 30 accurately centered reflections. The

reflections were selected between those with a higher intensity in the  $2\theta$  range between 14° and 32° and were measured in several equivalent positions on the diffractometer.

Intensity data up to  $\theta = 35^\circ$  were collected at 0.0001, 1.76, 2.81, 4.75, and 7.2 GPa, adopting nonbisecting geometry (Denner et al. 1978). Intensity data were analyzed with a digital procedure (Comodi et al. 1994) and visually inspected to eliminate errors resulting from an overlap of diffraction effects from some parts of the diamond cell and quartz or by shadowing from the gasket, and merged into an independent dataset. The data were corrected for pressure-cell absorption by an experimental attenuation curve (Finger and King 1978). Isotropic atomic displacement parameters were used for high-pressure refinements. Details of data collection, the results of the refinements, and structural parameters at high pressure are listed in Tables 1, 2, and 4.

## Results and discussion

### Structure refinement at ambient conditions

Rb–TFA is a 1M mica with a large unit-cell volume relative to common trioctahedral micas such as phlogopite (Table 4), owing to substitutions of Fe<sup>2+</sup> for magnesium, Fe<sup>3+</sup> for aluminum, and rubidium for potassium. Its structure is homo-octahedral, because the mean bond distances  $\langle M1-O \rangle$  are very near to  $\langle M2-O \rangle$  (Table 5) and because both M1 and M2 are occupied by divalent iron. The *C2/m* space group does not allow tetrahedral cation ordering. In addition to the composition indicated by the chemical analysis, the proportion of Fe<sup>3+</sup> and Si in tetrahedra was estimated from the mean bond length  $\langle T-O \rangle$  (1.687 Å) according to the equations of Weiss et al. (1992). The corresponding value for  $x_{Fe^{3+}}$  is 0.26, as expected if about 1/4 of the tetrahedral positions is occupied by Fe<sup>3+</sup>.

During the last stage of refinement, a difference Fourier synthesis showed some residuals which could be interpreted as due to the splitting of Rb and T positions into positions shifted by  $\mathbf{b}/3$ . This can be interpreted as a consequence of random stacking faults with a  $\mathbf{b}/3$  component. The presence of this kind of disorder is a common feature in micas (Brigatti and Davoli 1990 for biotite; Oberti et al. 1993 for preiswerkite; Mellini et al. 1996 for Cs-ferriannite). The stacking faults cause a shift of the interlayer and T cations, whereas M1 and M2 octahedral positions appear unaffected, being superimposed on the original ones. After the refinement, the occupancy of the “new” Rb and T positions shifted by

<sup>1</sup> Table 3 is deposited .....

**Table 2** Fractional atomic coordinates for Rb–TFA at different pressures,  $U_{eq}$  for all atoms in the refinement in air and for the Rb atom in DAC refinements,  $U_{iso}$  for all other atoms

| $P$ (GPa)           | Atom | $x/a$     | $y/b$      | $z/c$      | Ueq/Uiso  |
|---------------------|------|-----------|------------|------------|-----------|
| 0.0001 <sup>a</sup> | Rb   | 0         | 1/2        | 0          | 0.0317(3) |
|                     | M1   | 0         | 0          | 1/2        | 0.0121(3) |
|                     | M2   | 0         | 0.33215(8) | 1/2        | 0.0126(2) |
|                     | T    | 0.0766(1) | 0.1665(1)  | 0.22948(8) | 0.0139(3) |
|                     | O1   | 0.047(1)  | 0          | 0.1736(5)  | 0.0446(9) |
|                     | O2   | 0.3139(7) | 0.2443(5)  | 0.1740(3)  | 0.0445(9) |
|                     | O3   | 0.1308(5) | 0.1665(3)  | 0.3931(2)  | 0.0138(5) |
|                     | O4   | 0.1322(8) | 1/2        | 0.3988(4)  | 0.0158(8) |
| 0.0001 <sup>b</sup> | Rb   | 0         | 1/2        | 0          | 0.021(3)  |
|                     | M1   | 0         | 0          | 1/2        | 0.011(1)  |
|                     | M2   | 0         | 0.3321(4)  | 1/2        | 0.0115(8) |
|                     | T    | 0.0761(6) | 0.1665(4)  | 0.2291(7)  | 0.0152(9) |
|                     | O1   | 0.040(4)  | 0          | 0.172(4)   | 0.040(6)  |
|                     | O2   | 0.316(3)  | 0.243(1)   | 0.173(3)   | 0.037(4)  |
|                     | O3   | 0.131(2)  | 0.167(1)   | 0.391(2)   | 0.013(2)  |
|                     | O4   | 0.133(3)  | 1/2        | 0.410(3)   | 0.014(4)  |
| 1.76                | Rb   | 0         | 1/2        | 0          | 0.024(5)  |
|                     | M1   | 0         | 0          | 1/2        | 0.0096(9) |
|                     | M2   | 0         | 0.3328(3)  | 1/2        | 0.0102(8) |
|                     | T    | 0.0742(7) | 0.1664(3)  | 0.223(1)   | 0.0132(9) |
|                     | O1   | 0.033(4)  | 0          | 0.167(5)   | 0.040(5)  |
|                     | O2   | 0.317(3)  | 0.240(2)   | 0.165(4)   | 0.048(4)  |
|                     | O3   | 0.133(2)  | 0.1666(9)  | 0.401(4)   | 0.011(2)  |
|                     | O4   | 0.135(3)  | 1/2        | 0.395(4)   | 0.018(3)  |
| 2.81                | Rb   | 0         | 1/2        | 0          | 0.085(9)  |
|                     | M1   | 0         | 0          | 1/2        | 0.006(1)  |
|                     | M2   | 0         | 0.3328(3)  | 1/2        | 0.006(1)  |
|                     | T    | 0.075(1)  | 0.1661(5)  | 0.222(2)   | 0.018(1)  |
|                     | O1   | 0.021(7)  | 0          | 0.174(8)   | 0.063(9)  |
|                     | O2   | 0.318(5)  | 0.236(3)   | 0.152(5)   | 0.066(8)  |
|                     | O3   | 0.130(3)  | 0.164(1)   | 0.389(6)   | 0.011(4)  |
|                     | O4   | 0.122(3)  | 1/2        | 0.360(5)   | 0.002(4)  |
| 4.75                | Rb   | 0         | 1/2        | 0          | 0.153(9)  |
|                     | M1   | 0         | 0          | 1/2        | 0.011(2)  |
|                     | M2   | 0         | 0.3327(5)  | 1/2        | 0.011(1)  |
|                     | T    | 0.076(2)  | 0.1663(6)  | 0.227(3)   | 0.022(2)  |
|                     | O1   | 0.11(1)   | 0          | 0.18(2)    | 0.149(9)  |
|                     | O2   | 0.273(6)  | 0.263(4)   | 0.155(7)   | 0.064(9)  |
|                     | O3   | 0.144(5)  | 0.158(2)   | 0.417(9)   | 0.033(6)  |
|                     | O4   | 0.127(4)  | 1/2        | 0.366(6)   | 0.000(4)  |
| 7.2                 | Rb   | 0         | 1/2        | 0          | 0.146(9)  |
|                     | M1   | 0         | 0          | 1/2        | 0.015(3)  |
|                     | M2   | 0         | 0.334(1)   | 1/2        | 0.012(2)  |
|                     | T    | 0.068(3)  | 0.167(1)   | 0.211(5)   | 0.027(3)  |
|                     | O1   | 0.09(2)   | 0          | 0.17(2)    | 0.096(9)  |
|                     | O2   | 0.276(9)  | 0.271(6)   | 0.16(1)    | 0.076(9)  |
|                     | O3   | 0.129(5)  | 0.164(3)   | 0.39(1)    | 0.014(7)  |
|                     | O4   | 0.131(8)  | 1/2        | 0.372(9)   | 0.000(7)  |

<sup>a</sup> Data collected in air

<sup>b</sup> Data collected at room conditions in the DAC

**b**/3 converged to 8 and 10%, respectively, indicating the statistical frequency of the occurrence of stacking faults in the crystal. No allowance for the shift of oxygen atoms was made.

In the difference Fourier synthesis, the position of the H atom became evident, the O–H bond being perpendicular to the octahedral sheet and pointing toward the interlayer cation as in other trioctahedral micas. When H was included in the calculations, R converged to 0.025 for 749 observed reflections [ $I > 4\sigma(I)$ ] and 60 parameters.

The nearly identical dimensions of the tetrahedral and octahedral sheets allow a very small tetrahedral rotation angle  $\alpha$  [2.23(6)°]. The coordination polyhedron

around rubidium is very close to an ideal hexagonal prism with very small differences between “inner”, the six shortest, and “outer”, the six longest, Rb–O bonds (averaging 3.227 and 3.330 Å, respectively) (Table 5). The corrugation of the tetrahedral sheets ( $\Delta z$ ), is  $-0.003(9)$  Å (Table 5). Such a slight tilting is common in trioctahedral micas, because each tetrahedron shares its apical oxygen atom with three nearly identical octahedra, so the apical oxygen is not pulled one way or another. Let it be added that the octahedral flattening angle  $\psi$  (which is  $54^\circ 44'$  for an undistorted octahedron) is equal to  $59^\circ 12'$  in both M1 and M2 octahedra of the present mica; this is a value common to many trioctahedral micas.

**Table 4** Unit-cell parameters at different pressures

| $P$ (GPa)           | $a$ (Å)  | $b$ (Å)  | $c$ (Å)   | $\beta$ (Å) | $V$ (Å <sup>3</sup> ) |
|---------------------|----------|----------|-----------|-------------|-----------------------|
| 0.0001 <sup>a</sup> | 5.476(1) | 9.493(1) | 10.514(1) | 99.95(6)    | 538.3(1)              |
| 0.0001 <sup>b</sup> | 5.478(1) | 9.489(1) | 10.521(2) | 99.92(7)    | 538.7(3)              |
| 0.24                | 5.471(2) | 9.479(2) | 10.465(4) | 100.0(4)    | 534.5(5)              |
| 0.70                | 5.458(3) | 9.459(3) | 10.39(8)  | 100.1(6)    | 528.1(8)              |
| 1.00                | 5.448(4) | 9.445(3) | 10.345(4) | 100.0(6)    | 524.2(7)              |
| 1.51                | 5.438(2) | 9.429(2) | 10.302(6) | 100.1(5)    | 520.0(6)              |
| 1.76                | 5.442(3) | 9.435(2) | 10.185(4) | 100.3(4)    | 514.5(6)              |
| 2.81                | 5.412(2) | 9.392(2) | 10.120(4) | 100.2(4)    | 506.2(5)              |
| 3.36                | 5.408(2) | 9.385(2) | 10.062(9) | 100.3(3)    | 502.5(7)              |
| 3.84                | 5.412(2) | 9.396(2) | 9.967(4)  | 100.4(4)    | 498.6(5)              |
| 4.50                | 5.422(2) | 9.390(2) | 9.882(8)  | 100.7(5)    | 494.3(6)              |
| 4.75                | 5.420(2) | 9.383(2) | 9.846(6)  | 100.8(5)    | 491.9(5)              |
| 5.10                | 5.423(2) | 9.372(2) | 9.800(8)  | 100.6(6)    | 489.6(6)              |
| 5.40                | 5.423(3) | 9.360(2) | 9.760(8)  | 100.8(4)    | 486.7(8)              |
| 5.83                | 5.420(2) | 9.350(4) | 9.739(9)  | 100.6(4)    | 485.1(8)              |
| 6.28                | 5.416(2) | 9.343(4) | 9.731(8)  | 100.7(5)    | 483.9(7)              |
| 6.90                | 5.410(2) | 9.331(4) | 9.691(8)  | 100.7(5)    | 480.6(7)              |
| 7.06                | 5.411(4) | 9.329(3) | 9.668(8)  | 100.6(4)    | 479.7(7)              |
| 7.54                | 5.407(4) | 9.320(3) | 9.670(4)  | 100.7(4)    | 478.9(8)              |
| 7.20                | 5.410(4) | 9.325(3) | 9.645(6)  | 100.7(5)    | 478.1(8)              |
| 8.68                | 5.396(3) | 9.310(4) | 9.630(6)  | 100.8(6)    | 475.2(7)              |
| 9.61                | 5.379(3) | 9.310(3) | 9.585(6)  | 100.8(5)    | 471.5(7)              |
| 10.0                | 5.384(3) | 9.304(3) | 9.586(6)  | 100.8(5)    | 471.2(7)              |

<sup>a</sup> Data collected in air<sup>b</sup> Data collected under room conditions in the DAC

## Refinement at elevated pressures

Intensity data from crystals mounted in a DAC are always affected by systematic errors, because of various

interactions of the X-ray beams with the components of the cell. A restricted access to reflections results in a reduced resolution of the structure refinement and it is not safe to compare high-pressure structure refinements with those based on data collected from a crystal in air. Therefore, we compared the four refinements performed at 1.76, 2.81, 4.75, and 7.2 GPa with data collected at 0.0001 GPa, with the sample mounted in the DAC.

The results for 1.76 and 2.81 GPa are a gradual modification of the structure at ambient pressure (Table 5). As expected, the pressure-induced changes are more pronounced in the interlayer than in octahedral and tetrahedral sheets. Thus, the interlayer thickness drops from 3.58(2) Å (0.0001 GPa) to 3.18(4) Å (2.81 GPa) and there is a more pronounced differentiation between Rb–O<sub>inner</sub> and Rb–O<sub>outer</sub> with a concomitant decrease of the effective coordination number (from 11.9 to 10.7; Hoppe 1979). Parameters of octahedral and tetrahedral sheets change little or unsystematically, but there is a steady increase in the tetrahedral rotation angle  $\alpha$  from 3.08(8)° to 6.3(4)°.

However, the structures refined at 4.75 and 7.2 GPa are rather different. The plots of several variables against pressure show one kind of relationship for the low-pressure group (ambient to 2.81 GPa) and another for the high-pressure (4.75 and 7.2 GPa). Most display a break in slope between 2.81 and 4.75 GPa (Fig. 1), but the tetrahedral rotation angle displays a dramatic plunge

**Table 5** Interatomic distances (Å) and geometrical characteristics of polyhedra and their sheets

| $P$ (GPa)                         | 0.0001 <sup>a</sup> | 0.0001 <sup>b</sup> | 1.76      | 2.81      | 4.75      | 7.2       |
|-----------------------------------|---------------------|---------------------|-----------|-----------|-----------|-----------|
| Tetrahedra                        |                     |                     |           |           |           |           |
| T–O1                              | 1.685(2)            | 1.67(2)             | 1.67(2)   | 1.64(3)   | 1.65(4)   | 1.62(4)   |
| T–O2a                             | 1.684(4)            | 1.68(2)             | 1.70(2)   | 1.73(3)   | 1.66(4)   | 1.62(5)   |
| T–O2b                             | 1.684(4)            | 1.69(2)             | 1.67(2)   | 1.71(3)   | 1.79(4)   | 1.67(6)   |
| T–O3                              | 1.694(3)            | 1.69(2)             | 1.77(3)   | 1.67(4)   | 1.84(7)   | 1.73(7)   |
| $\langle$ T–O $\rangle$           | 1.687               | 1.68                | 1.70      | 1.69      | 1.73      | 1.66      |
| $V_T$ (Å <sup>3</sup> )           | 2.46(1)             | 2.4(1)              | 2.5(1)    | 2.4(1)    | 2.6(2)    | 2.3(2)    |
| $\Delta z$ (Å)                    | –0.003(9)           | –0.012(9)           | 0.02(1)   | 0.22(1)   | 0.23(1)   | 0.07(1)   |
| Sheet thickness (Å)               | 2.270(1)            | 2.26(1)             | 2.36(3)   | 2.29(4)   | 2.46(6)   | 2.17(4)   |
| Tetrahedral rotation $\alpha$ (°) | 2.23(6)             | 3.08(8)             | 4.3(2)    | 6.3(4)    | –7.5(5)   | –8.5(9)   |
| Octahedra                         |                     |                     |           |           |           |           |
| M1–O3 $\times$ 4                  | 2.134(3)            | 2.15(1)             | 2.07(2)   | 2.10(3)   | 1.93(4)   | 2.04(6)   |
| M1–O4 $\times$ 2                  | 2.109(4)            | 2.07(2)             | 2.08(3)   | 2.27(3)   | 2.20(3)   | 2.14(6)   |
| $\langle$ M1–O $\rangle$          | 2.126               | 2.12                | 2.07      | 2.16      | 2.02      | 2.07      |
| $V_{M1}$ (Å <sup>3</sup> )        | 12.56(6)            | 12.5(3)             | 11.5(4)   | 13.3(5)   | 10.4(6)   | 11.7(9)   |
| M2–O3a $\times$ 2                 | 2.128(3)            | 2.14(1)             | 2.07(2)   | 2.13(3)   | 2.05(4)   | 2.08(5)   |
| M2–O3b $\times$ 2                 | 2.137(3)            | 2.14(1)             | 2.07(2)   | 2.11(3)   | 1.95(4)   | 2.08(5)   |
| M2–O4 $\times$ 2                  | 2.112(3)            | 2.05(2)             | 2.11(2)   | 2.29(3)   | 2.24(3)   | 2.18(5)   |
| $\langle$ M2–O $\rangle$          | 2.126(2)            | 2.11                | 2.08      | 2.18      | 2.08      | 2.11      |
| $V_{M2}$ (Å <sup>3</sup> )        | 12.56               | 12.2(3)             | 11.6(3)   | 13.7(6)   | 11.2(6)   | 12.3(9)   |
| Sheet thickness (Å)               | 2.175(1)            | 2.13(1)             | 2.03(3)   | 2.39(3)   | 1.93(5)   | 2.16(4)   |
| Interlayer                        |                     |                     |           |           |           |           |
| Rb–O <sub>inner</sub> (Å)         | 3.227(6)            | 3.20(3)             | 3.09(3)   | 2.99(3)   | 3.32(3)   | 3.32(4)   |
| Rb–O <sub>outer</sub> (Å)         | 3.330(5)            | 3.34(2)             | 3.29(3)   | 3.29(3)   | 2.96(4)   | 2.92(4)   |
| $\langle$ Rb–O $\rangle$ (Å)      | 3.278               | 3.20                | 3.19      | 3.14      | 3.14      | 3.12      |
| Rb–MEFIR (Å) <sup>c</sup>         | 3.27                | 3.26                | 3.17      | 3.08      | 3.05      | 2.99      |
| Rb–ECoN <sup>c</sup>              | 11.9                | 11.8                | 11.5      | 10.7      | 10.1      | 9.6       |
| $V_{Rb}^{VI}$ (Å <sup>3</sup> )   | 44.712              | 43.8(2)             | 38.9(1.1) | 35.3(1.0) | 46.5(1.5) | 46.4(1.8) |
| $V_{Rb}^{XII}$ (Å <sup>3</sup> )  | 86.877              | 86.8(4)             | 65.8(1.8) | 65.1(1.9) | 65.2(2.2) | 62.9(2.4) |
| Interlayer thickness (Å)          | 3.601(3)            | 3.58(2)             | 3.32(3)   | 3.18(4)   | 3.15(7)   | 3.12(1)   |

<sup>a</sup> Data collected in air<sup>b</sup> Data collected under room conditions in the DAC<sup>c</sup> Mean fictive ionic radii (MEFIR) and effective coordination numbers (ECoN) were calculated according to Hoppe (1979)

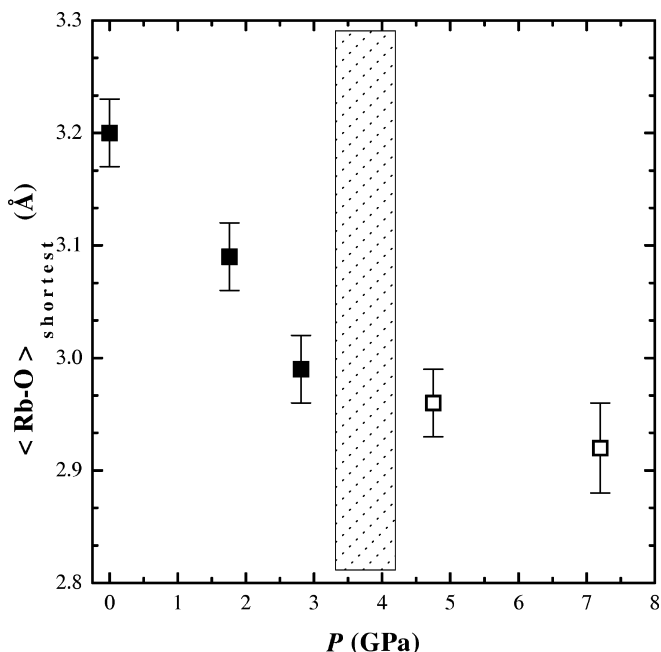


**Fig. 1** The mean of the six shortest bond Rb–O distances as a function of pressure. At 0.0001, 1.76, and 2.81 GPa these distances are the “inner” distances (*full squares*), whereas at 4.75 and 7.2 GPa they correspond to the “outer” ones (*open squares*). The *shaded area* represents the probable range of transition

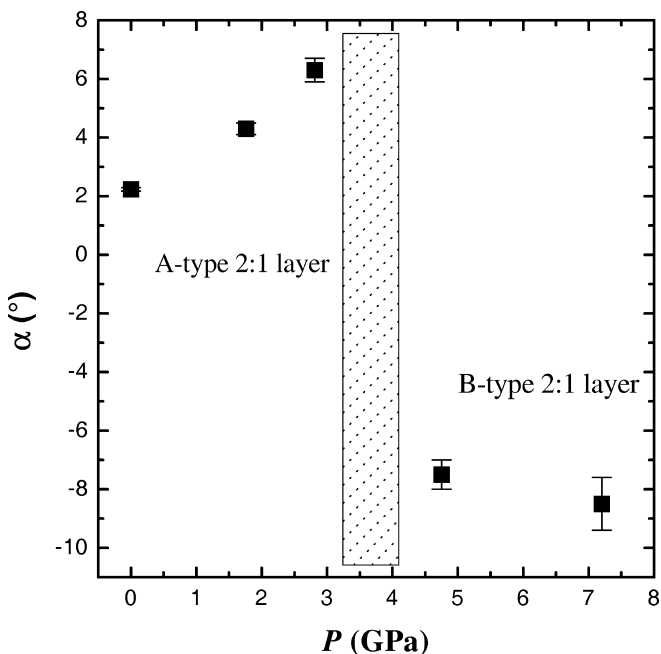


**Fig. 2** Tetrahedral rotation angle  $\alpha$  as a function of pressure. The *shaded area* represents the probable range of transition between Franzini A and B layers

from  $6.3(4)^\circ$  at 2.81 GPa to  $-7.5(5)^\circ$  at 4.75 GPa (Fig. 2). Meanwhile the six longest Rb–O distances at 0.0001, 1.76, and 2.81 GPa become the shortest at 4.75 and 7.2 GPa (Fig. 1).

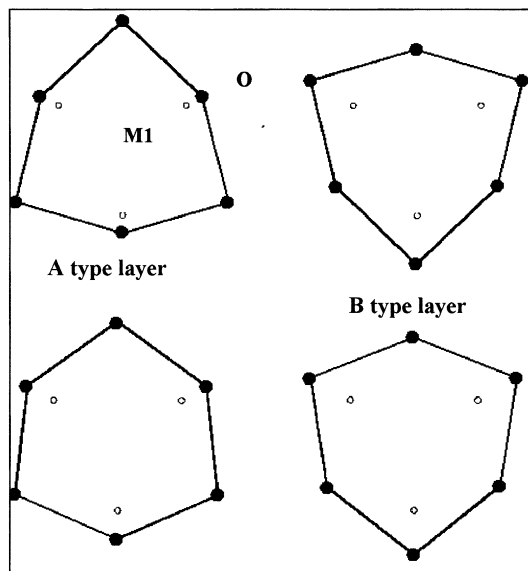


**Fig. 3** A schematic sketch illustrating the relation between Franzini A- and B-type layers: *Top drawings* shows Franzini's (1966,1969) construction of the A layer (*left*  $\alpha = 13.5^\circ$ ) and the B layer (*right*  $\alpha = -13.5^\circ$ ). *Bottom drawings* represent the structure of Rb–TFA (this study), the A layer at 2.81 GPa (*left*  $\alpha = 6.3^\circ$ ) and the B layer at 7.2 GPa (*right*  $\alpha = -8.5^\circ$ ). Only *outlines* of the ditrigonal rings of tetrahedra are shown; *open circles* represent octahedral cations; *dots* represent tetrahedral basal oxygen

**Table 6** Calculated energies for two Rb–TFA structure models at different pressures

| $P$ (GPa) | Franzini type | Energy (eV) |
|-----------|---------------|-------------|
| 0.0001    | A             | –633.3      |
| 2.8       | A             | –632.8      |
| 4.5       | A (simulated) | –613.5      |
| 4.5       | B             | –625.9      |

Negative tetrahedral rotation angle is the symptom of the B type of 2:1 layer predicted by Franzini (1966,1969). A and B structures are distinguished by two opposite ways of tetrahedral rotation that both accomplish an *ab* dimensional match between the tetrahedral and octahedral sheets. The rotation in which the triangles forming the tetrahedral bases and the octahedral triangular faces in the plane (001) point in opposite directions corresponds to the A-type structure (Fig. 3); the rotation in which they point in the same direction corresponds to the B-type structure.

In as much as the presently obtained rotation angles are unquestionably real and clearly above the error with which they are calculated, this is the first documented case of a Franzini B layer in the micas. The B-type layer has so far only been reported by Shirozu and Bailey (1965) for a chlorite. From an energetic point of view, the A-type structure in mica should be more stable than the B-type. In fact, the bridging oxygens in the A type partially shield interlayer cation from the octahedral cations.

**Fig. 4** Variation of the unit-cell parameters of Rb-TFA as a function of pressure. *Close squares* represent data collected at different pressure with the sample mounted in the DAC; *open triangles* represent data collected in air; *solid curves* represent the Birch–Murnaghan EoS best fit to the data up to 3.36 GPa

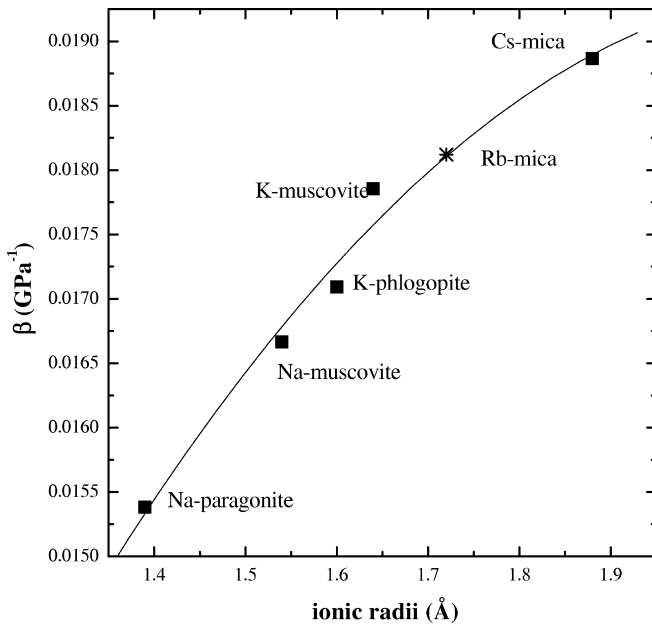
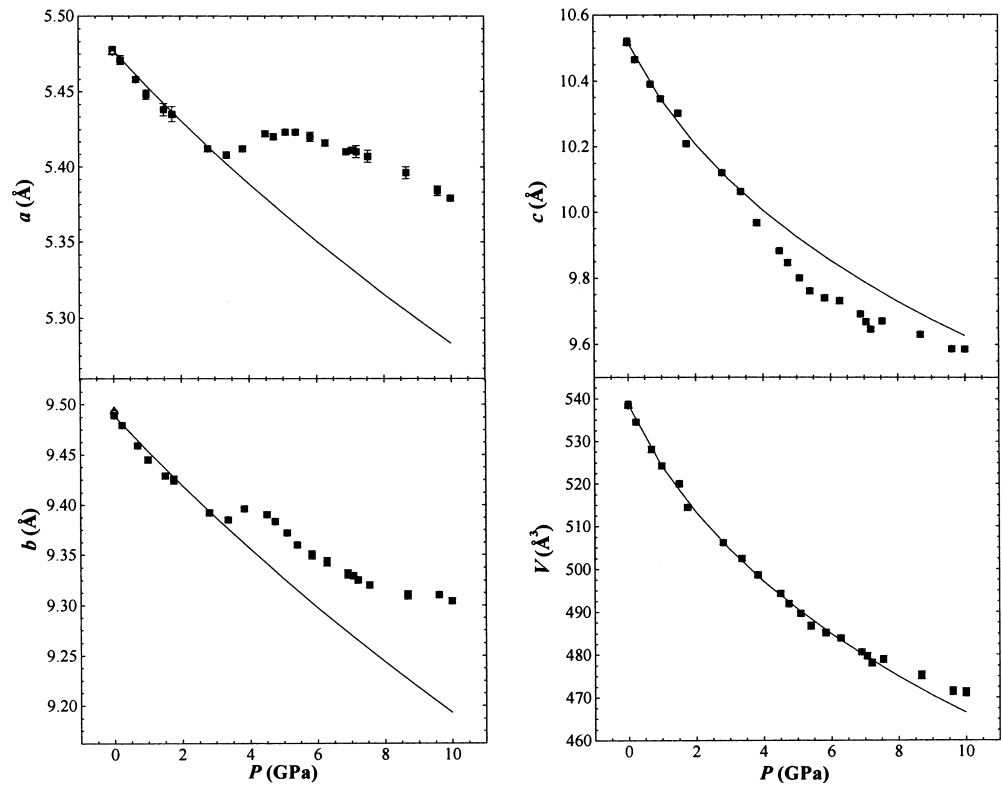


**Fig. 5** Mean compressibility coefficients of unit-cell volume for some micas vs. the ionic radius of the interlayer cation (radii from Shannon 1976). The ionic radii plotted are a mean reflecting the chemical composition (see text for references); the mean compressibility of the Rb-TFA shown is that of the “low-pressure” A-type structure

Semiquantitative computational simulation of the electrostatic energy for A- and B-type structures of Rb-TFA at different pressures was carried out to show

which structure will be preferred from an energetic point of view. For this purpose, the formalism coded in the computer program PARAPOCS (Parker and Price 1989), modified by Pavese et al. (1996), was used. Formal charges were assumed for the chemical species involved, whereas for solid solution a weighted mean was used. Even though their validity is qualitative, the results of the electrostatic energy calculations (Table 6) suggest that the type-A configuration is stable at pressures lower than 2.81 GPa. On the contrary, at 4.75 GPa and above, type B should be the preferred form.

From an energetic point of view, the discontinuity observed 2.8 and 4.5 GPa may be interpreted as an isosymmetric displacive phase transition from an A-type to a B-type structure. In this way, pressure-induced repulsion between tetrahedral and octahedral cations could be mitigated (Fig. 3) and at the same time the interlayer space could allow the accommodation of rubidium.

There appears to be little similarity in the behavior of Rb-TFA and other trioctahedral micas such as Cs-tetra-ferri-annite (Comodi et al. 1999) or phlogopite (Hazen and Finger 1978). In Rb-TFA, the tetrahedral rotation angle is significantly larger relative to Cs-tetra-ferri-annite: the latter exhibits only very small tetrahedral rotation angles,  $0.15^\circ$  at 0.0001 GPa and  $0.36^\circ$  at 3.94 GPa, and in heating experiments,  $\alpha$  refined as small and negative, between  $-0.14^\circ$  and  $-0.47^\circ$  for 296 and 435  $^\circ\text{C}$ , respectively. In phlogopite and other common trioctahedral K micas (all with Si, Al in

tetrahedra), the absence of a Franzini A–B transition can be ascribed to the small size of the interlayer cation; probably very high pressures (higher than those studied by Hazen and Finger 1978) would be required for it to take place.

### Compressibility and changes of unit-cell dimensions in pressure experiments

The specific response of the structure of the Rb–TFA to pressure, namely the discontinuity of the  $\alpha$  angle, indicates that the phase transition from A-type to B-type structure takes place somewhere between 2.81 and 4.75 GPa. To define more precisely the pressure at which the phase transition occurs, lattice parameters were measured at a number of pressures between room pressure and 10 GPa (Table 4). As can be seen in Fig. 4, the evolution of  $a$  and  $b$  parameters with pressure exhibits a sharp discontinuity above 3.36 GPa, whereas the discontinuity in the  $c$  parameter is less evident. The  $\beta$  angle increases linearly throughout the whole pressure range investigated. The evolution of the unit-cell volume with pressure seems continuous up to about 8 GPa, as the opposite responses of lattice parameters tend to cancel each other out.

We determined the compressibilities of lattice parameters by fitting the variation of lattice parameters with a Birch–Murnaghan equation of state (EoS) at pressure below the 3.36 GPa discontinuity (Fig. 4). The EoS order for each parameter was chosen from the analysis of the “normalized stress”,  $F_E$ , versus the finite strain  $f_E$  (Angel 2000). The results obtained are:  $a_0 = 5.478(1)\text{Å}$ ,  $K_0 = 74(3)\text{GPa}$ ;  $b_0 = 9.489(1)\text{Å}$ ,  $K_0 = 87(3)\text{GPa}$ , both with  $K'$  fixed at 4;  $c_0 = 10.521(1)\text{Å}$ ,  $K_0 = 17(2)\text{GPa}$  and  $K' = 6(2)$ ;  $V_0 = 538.7(1)\text{Å}^3$ ,  $K_0 = 31(3)\text{GPa}$  and  $K' = 13(4)$  from data up to 3.36 GPa.

These data show an anisotropic compressional pattern with the most evident pressure effect along the  $c$  axis ( $\beta_a:\beta_b:\beta_c = 1.2:1:5.1$ ), as observed in all phyllosilicates. In particular, the anisotropy is more pronounced in Cs-tetra-ferri-annite,  $\beta_a:\beta_b:\beta_c = 1:1.1:8.8$  (Comodi et al. 1999) and less pronounced in phlogopite, where  $\beta_a:\beta_b:\beta_c$  are 1:1.1:4.8 (Hazen and Finger 1978). In Fig. 6 the mean compressibility coefficients of the trioctahedral micas and those of some dioctahedral micas (muscovite, Na-muscovite, and paragonite; Comodi and Zanazzi 1995, 1997) are plotted against the ionic radius of the interlayer cation. The results point to a strong control of the interlayer cation over the bulk mica compressibility. Moreover, the homogeneous trend observed on a medley trioctahedral and dioctahedral micas suggests that the 2:1 layer plays only a secondary role in the whole compression behavior.

### Conclusions

1. The crystal structure of a synthetic Rb tetra-ferri-annite 1M with the composition  $\text{Rb}_{0.99}\text{Fe}^{2+}_{3.03}(\text{Fe}^{3+}_{1.04}\text{Si}_{2.96})\text{O}_{10.0}(\text{OH})_{2.0}$  is homooctahedral (space group  $C2/m$ ) with M1 and M2 occupied by divalent iron. Its unit cell is larger than that of the common potassium trioctahedral mica and similar lateral dimensions of the tetrahedral and octahedral sheets allow a small tetrahedral rotation angle  $\alpha = 2.23(6)^\circ$ .
2. Structure refinements at 0.0001, 1.76, 2.81, 4.75, and 7.2 GPa (in a DAC) indicate that the octahedra of Rb–TFA are more compressible than the tetrahedra and the interlayer is four times more compressible than the 2:1 layer. However, there is a peculiar behavior of the tetrahedral rotation angle  $\alpha$ : at lower pressures (0.0001, 1.76, 2.81 GPa), it is positive and increasing with pressure [from  $3.08(8)^\circ$  to  $6.3(4)^\circ$ ] as in other micas, but negative values  $-7.5(5)^\circ$  and  $-8.5(9)^\circ$  appear at higher pressures, 4.75 and 7.2 GPa, respectively. This structural evidence, together with electrostatic energy calculations, shows that the Rb–TFA has a Franzini A-type 2:1 layer up to at least 2.81 GPa that at higher pressure yields to a B-type layer, as shown by the refinements at 4.75 and 7.2 GPa.
3. The unit-cell data of Rb–TFA measured at 25 different pressures between 0.0001 and 10 GPa show a discontinuity in the evolution of all parameters above 3.36 GPa. Compressibility data are:  $a_0 = 5.478(1)\text{Å}$ ,  $K_0 = 74(3)\text{GPa}$ ;  $b_0 = 9.489(1)\text{Å}$ ,  $K_0 = 87(3)\text{GPa}$  ( $K'$  fixed at 4 for  $a_0$  and  $b_0$ );  $c_0 = 10.521(1)\text{Å}$ ,  $K_0 = 17(2)\text{GPa}$  and  $K' = 6(2)$ ;  $V_0 = 538.7(1)\text{Å}^3$ ,  $K_0 = 31(3)\text{GPa}$ , and  $K' = 13(4)$ , from measurements up to 3.36 GPa.
4. On the basis of the evolution of the unit-cell parameters, the A–B transition in the Rb–TFA takes place between 3.36 and 3.84 GPa.

**Acknowledgements** We thank Alessandro Pavese for his contribution to the energetic calculations on the Rb–TFA structure. Many thanks are due to H.A. Giles (MA) for editing the English of the paper. This work was financially supported by CNR and MURST. (project Trasformazioni, reazioni, ordinamenti nei minerali) grants to P.F. Zanazzi.

### References

- Angel RJ (2000) Equations of State. High-Pressure and High-Temperature Crystal Chemistry. In: Hazen RM, Downs RT (eds) Reviews of Mineralogy and Geochemistry. Min Soc Am Vol 41, pp 35–59, Washington, DC, USA
- Angel RJ, Allan DR, Miletich R, Finger LW (1997) The use of the quartz as an internal pressure standard in high-pressure crystallography. *J Appl Crystallogr* 30:461–466
- Brigatti MF, Davoli P (1990) Crystal structure refinements of 1 M plutonic biotites. *Am Mineral* 75:305–313

- Comodi P, Zanazzi PF (1993) Improved calibration curve for the  $\text{Sm}^{2+}$ : BaFCl pressure sensor. *J Appl Crystallogr* 26:843–845
- Comodi P, Zanazzi PF (1995) High-pressure structural study of muscovite. *Phys Chem Miner* 22:170–177
- Comodi P, Zanazzi PF (1997) Pressure dependence of structural parameters of paragonite. *Phys Chem Miner* 24:274–280
- Comodi P, Melacci PT, Polidori G, Zanazzi PF (1994) Trattamento del profilo di diffrazione da campioni in cella ad alta pressione. Proceedings of XXIV National Congress of Associazione Italiana di Cristallografia. Pavia, Sept 27–29, pp 119–120
- Comodi P, Zanazzi PF, Weiss Z, Rieder M, Drábek M (1999) “Cs-tetra-ferri-annite:” high-pressure and high-temperature behavior of a potential nuclear waste disposal phase. *Am Mineral* 84:325–332
- Denner W, Schultz H, D’Amour H. (1978) A new measuring procedure for data collection with a high-pressure cell on an X-ray four-circle diffractometer. *J Appl Crystallogr* 11:260–264
- Drábek M, Rieder M, Viti C, Weiss Z, Fryda J (1998) Hydrothermal synthesis of a Cs ferruginous trioctahedral mica. *Can Mineral* 36:755–761
- Finger LW, King H (1978) A revised method of operation of the single-crystal diamond cell and refinement of the structure of NaCl at 32 kbar. *Am Mineral* 63:337–342
- Franzini M (1966) Nuovi dati sulla struttura delle miche triottedriche. *Atti Soc Tosc Sci Nat Mem (A)* LXXIII:620–631
- Franzini M (1969) The A and B mica layer and the crystal structure of sheet silicates. *Contrib Mineral Petrol* 21:203–224
- Hazen RM, Finger LW (1978) The crystal structure and compressibilities of layer minerals at high pressure. II Phlogopite and Chlorite. *Am Mineral* 63:293–296
- Hoppe R (1979) Effective coordination numbers (EcoN) and mean fictive ionic radii (MEFIR). *Z Kristallogr* 150:23–52
- Ibers JA, Hamilton WC (eds) (1974) International tables for X-ray crystallography, vol 4, Knoch, Birmingham, UK pp 99–101
- Mellini M, Weiss Z, Rieder M, Drábek M (1996) Cs-ferriannite as a possible host for waste cesium: crystal structure and synthesis. *Eur J Mineral* 8:1265–1271
- North ACT, Philips DC, Matthews FS (1968) A semiempirical method of absorption correction. *Acta Crystallogr (A)*24:351–359
- Oberti R, Ungaretti L, Tlili A, Smith DC, Robert JL (1993) The crystal structure of preiswerkite. *Am Mineral* 78:1290–1298
- Parker SC, Price GD (1989) Computer modeling of phase transition in minerals. *Adv Sol State Chem* 1:295–327
- Pavese A, Catti M, Parker S, Walls A (1996) Modelling of thermal dependence of elastic properties in calcite ( $\text{CaCO}_3$ ). *Phys Chem Miner* 23:89–93
- Shannon RD (1976) Revised effective ionic radii and systematic study of interatomic distances in halides and chalcogenides. *Acta Crystallogr (A)*32:751–767
- Sheldrick GM (1997) SHELX-97. Program for crystal structure determination. University of Göttingen, Germany
- Shirozu H, Bailey SW (1965) Chlorite polytypism: III. Crystal structure of an orthohexagonal iron chlorite. *Am Mineral* 50:868–885
- Weiss Z, Rieder M, Chmielová M (1992) Deformation of coordination polyhedra and their sheets in phyllosilicates. *Eur J Mineral* 4:665–682